A Comparison of numerical simulation models for predicting temperature in solidification analysis with reference to air gap formation

J. Kron, Michel Bellet, Andreas Ludwig, Bjorn Pustal, Joachim Wendt, Hasse Fredriksson

Int. J. Cast Metals Research 17 (2004) 295-310

A Comparison of Numerical Simulation Models for Predicting Temperature in Solidification Analysis with Reference to Air Gap Formation

J. KRON, M. BELLET[#], A. LUDWIG, B. PUSTAL,

J. WENDT and H. FREDRIKSSON

ABSTRACT

Due to its influence on the heat transfer between cast part and mould the air gap formation is an important problem for many casting processes. The general explanation for the gap formation is that as a result of stresses and distortions that are created from inhomogeneous cooling, shrinkage of the casting and expansion of the mould occurs. In this paper we apply different thermomechanical approaches by using three commercial and one in-house code to a well defined casting process and compare their predictions with experimental findings. The experimental facts were gained from the solidification and subsequent cooling of cylindrical castings of eutectic Al-13%Si and ternary Al-7%Si-0.3%Mg alloys. Based on these findings, the major differences between the predictions of the models and the actual formation of the air gap are discussed.

[#]Correspondence to: Michel Bellet, Centre de Mise en Forme des Matériaux, Ecole des Mines de Paris, UMR CNRS 7635, BP 207, 06904 Sophia Antipolis, France.

J. Kron, PhD student, and H. Fredriksson, full professor, are with the KTH Stockholm, Sweden. M. Bellet, senior scientist, is with Ecole des Mines de Paris, Centre for Material Processing (CEMEF), Sophia Antipolis, France. A. Ludwig, full professor, is with the University of Leoben, Department of Metallurgy, Austria. B. Pustal, PhD student, is with the Foundry Institute of the Aachen University, Germany. J. Wendt was senior research scientist at VTT Industrial Systems, Espoo, Finland, during the study and is now with RWP GmbH, Roetgen, Germany.

NOTATIONS

c_p	specific heat ($J.kg^{-1}.K^{-1}$)
E	Young modulus (Pa)
f_s	volumetric solid fraction (-)
h	heat transfer coefficient (HTC) ($W.m^{-2}.K^{-1}$)
$\bar{\bar{I}}$	identity tensor (-)
m	strain-rate sensitivity index (-)
$p = -\frac{1}{3}\,\mathrm{tr}\,\bar{\bar{\sigma}}$	pressure (Pa)
$\bar{\bar{s}} = \bar{\bar{\sigma}} + p\bar{\bar{I}}$	deviatoric stress tensor (Pa)
T	temperature (K or °C)
T_S	solidus temperature (K or °C)
T_L	liquidus temperature (K or °C)
α	thermal linear expansion coefficient (K^{-1})
Δh_f	specific latent heat of fusion ($J.kg^{-1}$)
$\Delta\varepsilon^{tr} = \frac{\rho(T_L) - \rho(T_S)}{\rho(T_L)} < 0$	shrinkage ratio : relative volume change associated with the total liquid-solid transition (-)
$\bar{\bar{\dot{\varepsilon}}}$	strain rate tensor (s^{-1})
$\bar{\bar{\dot{\varepsilon}}}^{el}$	elastic part of the strain rate tensor (s^{-1})
$\bar{\bar{\dot{\varepsilon}}}^{pl}$	plastic part of the strain rate tensor (s^{-1})
$\bar{\bar{\dot{\varepsilon}}}^{vp}$	viscoplastic part of the strain rate tensor (s^{-1})
$\bar{\bar{\dot{\varepsilon}}}^{th}$	thermal part of the strain rate tensor (s^{-1})
$\dot{\varepsilon}_{eq}^{pl} = \sqrt{\frac{2}{3}\dot{\varepsilon}_{ij}^{pl}\dot{\varepsilon}_{ij}^{pl}}$	von Mises equivalent plastic (or viscoplastic: *vp* instead of *pl*) strain-rate (s^{-1})
$\dot{\varepsilon}_{eq} = \sqrt{\frac{2}{3}\dot{\varepsilon}_{ij}\dot{\varepsilon}_{ij}}$	von Mises equivalent strain-rate (s^{-1})
$\varepsilon_{eq}^{pl} = \int_0^t \dot{\varepsilon}_{eq}^{pl}\,dt$	von Mises equivalent plastic (or viscoplastic: *vp* instead of *pl*) strain (-)

$\varepsilon_{eq} = \int_0^t \dot{\varepsilon}_{eq} dt$	von Mises equivalent strain (-)
λ	thermal conductivity ($W.m^{-1}.K^{-1}$)
ν	Poisson coefficient (-)
ρ	specific mass ($kg.m^{-3}$)
$\overline{\overline{\sigma}}$	Cauchy stress tensor (Pa)
$\sigma_{eq} = \sqrt{\frac{3}{2} s_{ij} s_{ij}}$	von Mises equivalent stress (Pa)
σ_y	static yield stress (Pa) (plastic threshold : if $\sigma_{eq} < \sigma_y$, the material is elastic)

INTRODUCTION

Air gap formation is an important problem in many casting processes since it has a large influence on the heat transfer between casting and mould. Work on the connection between varying heat transfer coefficient and the formation of an air gap has been presented in various articles about mould casting [1-6]. The gap formation has been found to start when the solid metal shell is strong enough to resist the pressure from the liquid metal [7]. The heat transfer from the metal to the mould is dominated by conduction before an air gap has formed. When a macroscopic air gap is formed the conduction is reduced and the heat transfer could be described as the sum of the conduction and the radiation over the slit [8]. In the case of aluminium base alloys the heat transfer due to radiation is insignificant [9]. Convection has been proved to have a negligible effect [10]. The general explanation of the air gap formation is that shrinkage of the casting and expansion of the mould occur due to stresses and strains from thermal gradients created during the casting process [10-15].

In mathematical modelling of a casting process, governing equations, thermophysical properties and boundary conditions are needed. For most practical casting processes the thermal boundary conditions are difficult to decide thoroughly for all points of the mould/metal interface. The reason for this is that the heat transfer can vary considerably with time and temperature along the face of the casting. Still these boundary conditions decide the results of thermal as well as thermomechanical modelling of the process.

In the present work experiments have been done where temperatures and displacements of the casting and the mould have been measured during a solidification process. The geometry of the set-up has been chosen to be of a simple cylindrical shape in order to make it possible to deduce a heat transfer coefficient from the temperature measurements that is valid for the whole boundary of the casting.

The aim of the present work is to model the experiment described above numerically with the calculated heat transfer coefficient as a boundary condition. The different thermomechanical approaches used by four different simulation programs should be used in the modelling work. The results of the modelling predictions regarding the solidification process as well as the displacements forming an air gap should be compared to each other and to the experimental results. The simulation programs used here were CASTS-SPAN3D [16], MAGMASOFT [17], PROCAST [18] and THERCAST [19].

The alloys chosen for the experiments were eutectic Al-13%Si (non-modified) and Al-7%Si-0.3%Mg (not grain refined). Simulation work has earlier been done in this area [11, 12], based on experiments performed earlier by P. Schmidt and I.L. Svensson [20]. However, in their work, only the total air gap was given, the thermal expansion of the mould was not distinguished from the contraction of the casting.

1. EXPERIMENTAL DESCRIPTION AND RESULTS

A series of casting experiments have been performed in a cylindrical mould with a core in its centre. The height of the mould was 100 mm, and the external diameters of the core, the

casting and the mould were 24, 150 and 250 mm, respectively. A geometric description of the experimental set-up is shown in Figure 1.

The mould was made from a low alloy steel (0.14% C, 0.35% Si and 1.2% Mn) and the core was made as a quartz tube filled with oil bound sand. The bottom and the top of the core, casting and mould were insulated. Five thermocouples of type K were inserted in the mould and four in the casting, all aligned at mid height of the set-up. In the mould the radial distance between the thermocouples was about 10 mm and in the melt 15 mm. Cooling curves were recorded throughout the solidification process and the subsequent cooling.

Two types of experiments were performed: one with eutectic Al-13%Si and the other with Al-7%Si-0.3%Mg as cast alloys. The series of experiments performed with eutectic Al-13%Si as cast alloy have been presented earlier and additional experiment series with other alloys have been done [21, 22]. The melt was poured from the top of the mould and the upper surface was rapidly covered with granulated insulating material. The initial temperature of the mould was 117 °C and 130 °C for Al-13%Si and Al-7%Si-0.3%Mg respectively. The estimated initial temperature after filling was 779 °C and 716 °C for Al-13%Si and Al-7%Si-0.3%Mg respectively.

Figure 2 shows the cooling curves from the experiments of the two alloys. In the figure only two from nine recorded temperature curves are displayed; one taken in the mould and the other in the casting.

The displacements of the mould and the casting were measured with linear variable differential transducers (LVDT's), placed according to Figure 1. Quartz tubes have been used to connect the LVDT's to the measuring points. The quartz tubes froze into the solidifying shell and followed it as it moved. The movement of the inner mould wall was measured at a distance of 1 mm from the inner mould surface. The size of the air gap was then determined as the difference between the movements of the solid metal shell and the inner wall of the mould. To assure that the displacements occur symmetrically they were measured at three locations around the cylinder with 120° in between. This kind of experiment does not always show a good symmetry, only about one out of three experiments was symmetrical. Experiments that did not show symmetric behaviour were always discarded since the measured heat transfer would not be applicable to the whole boundary of the casting otherwise. A maximum difference of 20 μm was accepted in the displacement measurements. In Figure 3 the experimentally measured displacements, and consequently air gaps, are shown for the two experiments presented here. It is worth noting that the row of thermocouples was placed in the vicinities of the measuring points for the displacement.

The heat transfer coefficient (HTC) at the interface between casting and mould, h, was derived from the knowledge of heat fluxes in the vicinity of the interface. The mathematical expression used to estimate h from the measured temperatures is given as:

$$-\lambda_{casting} \cdot \left(\frac{\partial T}{\partial r}\right)_{casting} = h \cdot (T_{i,casting} - T_{i,mould}) = -\lambda_{mould} \cdot \left(\frac{\partial T}{\partial r}\right)_{mould} \quad (1)$$

where $\lambda_{casting}$ and λ_{mould} are the heat conductivities of the casting and the mould and $T_{i,casting}$ and $T_{i,mould}$ are the interface temperatures of the casting and the mould. The interface temperatures in the mould and the casting were extrapolated from a third order polynomial fitting of the measured temperatures. The temperature gradient at the surface of the mould must also be known in order to calculate the heat transfer coefficient. The temperature gradient was taken as the derivative of the fitted polynomial at the surface of the mould. The heat transfer coefficients deduced with this method from the measured temperature distribution are given in Figure 4.

2. NUMERICAL SIMULATION

2.1. Basic Considerations and Definition of the Problem

2.1.1. Geometrical description

In the modelling work the initial dimensions of the geometry are as given in Section 1. Four different computational domains are identified: i) core, ii) metal (casting); (iii) mould and (iv) insulation. Time and spatial discretisations have not been imposed. Finite differences and finite element meshes have been used, depending on the software. Full three-dimensional meshes or meshes of a restricted angular sector have been used. Details are given in Section 2.2 for each software application.

2.1.2. Three different types of calculations

The benchmarking exercise has been conducted in three steps:

- **Step 1: Pure heat transfer calculation with constant heat transfer coefficients**. This preliminary step serves as a comparison between the heat transfer solvers of the different numerical codes. The whole model is considered rigid. The influence of the air gap on the cooling of the specimen is neglected.
- **Step 2: Thermo-mechanical calculation with time dependent HTC between the part and the external mould**. The solidifying part and the mould deform. The core and the insulation are assumed rigid. The time dependent HTC is deduced from the experiments, as explained in Section 1. So, there is no effective coupling from the mechanical calculation towards the heat transfer calculation. Only the coupling from the thermal calculation towards the mechanical calculation is taken into account through the temperature dependency of the part and mould constitutive parameters.
- **Step 3: Thermo-mechanical calculation with gap dependent HTC between the part and the external mould**. As in step 2, the solidifying part and the mould deform. The core and the insulation are assumed rigid. However, in this case the full thermomechanical coupling is considered, since the HTC directly depends on the gap thickness, which is a result from the mechanical calculation.

2.1.3. Materials properties

For the numerical simulation of the cylinder experiments four material groups were considered: i) core, ii) metal (casting); (iii) mould and (iv) insulation. For the thermal description of the process the following material properties had to be agreed on: heat conductivity, $\lambda(T)$, specific mass, $\rho(T)$, and specific heat, $c_p(T)$. Additionally, the latent heat of fusion, Δh_f, the evolution of solid fraction, $f_s(T)$, and the liquidus and solidus temperatures, T_L and T_S, have to be known for the cast metal. For the metal and the mould we agreed on temperature dependent properties, whereas for the core and the insulation we used constant ones[1]. Note that if the release of the latent heat is modelled via Δh_f and $f_s(T)$ the values of $c_p(T)$ should not contain any contribution of the latent heat.

Although the core is encased with a quartz tube, it is modelled entirely by using sand properties.

For the mechanical computation the following material properties were compiled: Young's modulus, $E(T)$, Poisson's ratio, $\nu(T)$, thermal expansion coefficient, $\alpha(T)$, and yield stress, $\sigma_y(T)$. If needed, the linear thermal expansion coefficient $\alpha(T)$ and the relative volumetric solidification shrinkage, $\Delta\varepsilon^{tr}$ were deduced from the primary data $\rho(T)$.

In the different approaches associated with the different codes presented in Section 2.2, it is assumed that the material behaves elastically if the von Mises equivalent stress σ_{eq} is smaller than the yield stress σ_y. If σ_{eq} exceeds σ_y, it is assumed that, depending on the model, the material behaves either plastically or visco-plastically:

$$\begin{aligned} &\sigma_{eq} < \sigma_y \quad \text{elastic behaviour} \\ &\sigma_{eq} > \sigma_y \quad \text{elastic - plastic or elastic - visco - plastic behaviour} \end{aligned} . \tag{2}$$

To describe the stress/strain curve above the yield stress it was assumed that the elastic-plastic Ramberg-Osgood stress-strain model [23, 24] can be applied. Although the deformation of liquid, semi-solid and high temperature solid-state metallic alloys is obviously strain-rate dependent, this choice has been done in order to be able to compare the different numerical codes by using a common constitutive model that the four numerical codes used in this study can address. Thus, in the plastic regime stress and (reference) strain is related by

$$\left[\frac{\sigma_{eq}}{\sigma_y}\right]^n = 1 + n \cdot \left(\frac{\varepsilon_{eq}}{\varepsilon_y} - 1\right) \quad \text{for } \varepsilon_{eq} \geq \varepsilon_y . \tag{3}$$

Here, $\varepsilon_y = \sigma_y / E$ is the maximum elastic strain. Obviously, the reference strain ε_{eq} represents the total strain, that is the sum of the elastic and the (visco-)plastic strain. The dimensionless parameter $n(T)$ behaves like the inverse of a strain hardening coefficient. For $n = 1$, Eq. (3) turns into Hooke's law and shows only elastic behaviour, whereas for $n = \infty$, the material approaches ideal plasticity (σ_{eq} is close to σ_y, whatever the value of ε_{eq}). As the different numerical codes use different stress-strain models, the constitutive information given

[1] All materials properties used in this study can be made available by the authors.

by Eq. (3) must be transferred in the model used by the corresponding programs. The procedure will be described together with the description of each numerical code.

2.1.4. Initial conditions

The major objectives of this work are the simulation of the gap that forms between the cylindrical casting and the mould by using different approaches and to compare the prediction with experimental findings. We decided not to overload the task by simulating the mould filling. Thus, it is assumed, as already indicated in Section 1, that the process starts by cooling of melt with a uniform temperature distribution in a preheated assembly of the mould, the core and the insulation having the same initial temperature.

2.1.5. Boundary conditions

As outer thermal boundary condition we assume a constant HTC of h_{out} = 20 W.m^{-2}.K^{-1} between mould, insulation and surrounding. The temperature of the surrounding was assumed to be T_{out} = 20 °C.

Between each pair of materials from core, metal, mould, and insulation we assume the existence of a heat transfer coefficient. Those HTCs were chosen either to be constant, time dependent or dependent on any gap which forms between the materials.

The HTC between part and core is assumed to be constant, $h_{casting/core}$ = 2000 W.m^{-2}.K^{-1}. It can be shown that this assumption has a negligible influence on the results since the core rapidly reaches the temperature of the melt.

The heat exchange coefficient with insulation has been fixed to an arbitrary value, $h_{*/insulation}$ = 400 W.m^{-2}.K^{-1} ($*$ stands for casting, mould and core).

Heat transfer coefficient between part and mould

Although the assumption of a constant value of the HTC between the casting and the mould is unrealistic in this case, it enables a comparison of the codes on a very fundamental level. This is the objective of the calculations conducted in step 1. We have chosen the constant values given in Table 1. Those values correspond to the maximum values measured in the experiment before the gap forms, as illustrated by Figures 4A and B.

2.2. Presentation of the different numerical models

2.2.1. CASTS-SPAN3D:

CASTS is an in-house finite element code for casting simulations originally written at the Foundry Institute of the Aachen University. However, since the early times of CASTS many features have been added by ACCESS Materials and Processes e.V., a non-profit Institute founded by the Foundry Institute in 1986. The calculations in the frame of the present project have been done with version 12.6 [16].

Parallel to the development of CASTS a numerical code to simulate stresses and distortions during solidification and cooling of cast parts, SPAN3D, has been written at the Foundry Institute [25]. This software code uses result files, namely temperature solutions, from e.g.

CASTS in order to predict stresses and distortions caused by an inhomogeneous cooling. As long as a sequence of files with temperature results is available, SPAN3D can be used completely independent of CASTS. It may predict stresses and distortions for any material classes desired; mould, core or casting or for all three. However, if two materials are chosen which are initially in contact, SPAN3D considers the two materials to be in permanent contact. Therefore, only the deformation of the casting has been simulated.

Main features of the mechanical code SPAN3D

The calculation of stresses and deformations is based upon a thermo-elastic-plastic model. The equations are derived from the Prandtl-Reuss equations and are written as follows:

$$\begin{cases} \dot{\bar{\bar{\varepsilon}}} = \dot{\bar{\bar{\varepsilon}}}^{el} + \dot{\bar{\bar{\varepsilon}}}^{pl} + \dot{\bar{\bar{\varepsilon}}}^{th} \\ \dot{\bar{\bar{\varepsilon}}}^{el} = \dfrac{1+\nu}{E}\dot{\bar{\bar{\sigma}}} - \dfrac{\nu}{E}\mathrm{tr}(\dot{\bar{\bar{\sigma}}})\bar{\bar{I}} + \dot{T}\dfrac{\partial}{\partial T}\left(\dfrac{1+\nu}{E}\right)\bar{\bar{\sigma}} - \dot{T}\dfrac{\partial}{\partial T}\left(\dfrac{\nu}{E}\right)\mathrm{tr}(\bar{\bar{\sigma}})\bar{\bar{I}} \\ f = \sigma_{eq} - \sigma_y \le 0 \\ \dot{\bar{\bar{\varepsilon}}}^{pl} = \dfrac{3\dot{\varepsilon}_{eq}}{2\sigma_{eq}}\bar{\bar{s}} \quad \text{if} \quad f = 0 \text{ and } \bar{\bar{s}} : \dot{\bar{\bar{\sigma}}} \ge 0 \qquad \text{and} \qquad \dot{\bar{\bar{\varepsilon}}}^{pl} = 0 \quad \text{otherwise} \\ \dot{\bar{\bar{\varepsilon}}}^{th} = \alpha\dot{T}\bar{\bar{I}} \end{cases} \tag{4}$$

In the second equation, the two last terms account for the temperature dependency of elasticity coefficients E and ν. The third equation is the condition imposed by the von Mises plasticity criterion. The yield stress σ_y can vary with the plastic deformation ε_{eq}^{pl} according to a linear strain hardening model. The fourth equation is the von Mises'plastic flow rule.

Application of CASTS-SPAN3D to the benchmark test

For the four material groups mould, casting, core and insulations a three-dimensional FEM grid covering one quarter of the full model was designed, using 18360 hexahedra, 1008 pentahedra and 23741 nodes. The corresponding characteristic size of the elements is about 4.5 mm. For the thermal simulation a constant time step Δt = 0.5 s was used. The subsequent decoupled simulation of stresses and distortions were performed with Δt = 1 s.

The shrinkage is described by a modified thermal expansion coefficient. In the solidification interval, the value of α in the fourth equation of (4) is chosen such that:

$$3\alpha(T_L - T_S) = -\Delta\varepsilon^{tr} \tag{5}$$

where $\Delta\varepsilon^{tr}$ is the shrinkage ratio associated with the solidification.

2.2.2. MAGMASOFT:

MAGMASOFT® is a 3-D commercial simulation software based on the finite difference method. It is composed of several modules for different purposes like calculations of stresses and distortions, macrosegregation, and microstructure predictions for example. There is also a database available in the program.

Main features of the stress module of MAGMASOFT

MAGMAstress is the module used by MAGMASOFT for calculations of stresses and distortions formed in a solidification process. The program makes thermal calculations first and uses the calculated temperature distribution as in-data for MAGMAstress. The thermal and the thermomechanical calculations could not be coupled.

For the stress simulation a thermo-elastic-plastic model is considered. It is based on the same equations as (4). The following material properties are available in the database of MAGMASOFT: Young's modulus, Poisson's coefficient, thermal expansion coefficient, yield stress and coefficients of strain hardening.

Application of MAGMASOFT to the benchmark test

The MAGMAstress version 4.0 was used in this work. For the four material groups defined; mould, casting, core, and insulation, the full geometrical model was discretised with a grid using 606528 volume elements. 119040 of these volumes were used for the casting (average characteristic size 2.4 mm). For the thermal simulation automatic time step controlling is applied.

Since coupled temperature-stress calculations are not possible in MAGMASOFT the temperature distribution was calculated first, followed by a calculation of stresses and distortions. This subsequent simulation was performed with a maximum time step of 20 seconds. The shrinkage was described by a modified thermal expansion coefficient, like in CASTS-SPAN3D: see Section 2.2.1.

The program does not give the possibility to calculate displacements in two connected materials simultaneously. Therefore the calculation of an air gap had to be made in two steps; one where the displacement of the casting was calculated, and one where the displacement of the mould was calculated.

2.2.3. PROCAST

PROCAST™ is a commercial finite element software package for casting simulation. The code is developed by the company UES [26]. It consists of one base module and seven optional modules. The Base Module consists of a solidification solver with pre and post processors. The additional modules are Meshing, Fluid, Stress, Radiation, Microstructure, Electromagnetic, and Inverse.

Main features of the thermomechanical module of PROCAST

The module accounts for transient, non-linear 3D heat conduction, heat convection and radiation, with phase changes treated using an enthalpy formulation. The heat exchange between facing domains can be treated with coincident or non-coincident meshes.

Heat transfer and stress calculations are coupled. Thermal contact between parts is considered by means of an effective HTC, h_{eff}, which is defined as

$$h_{eff} = \frac{1}{\frac{1}{h_0} + \frac{1}{h_{air} + h_{rad}}} \quad \text{with} \quad h_{air} = \frac{\lambda_{air}}{g} \tag{6}$$

λ_{air} being the conductivity of air (zero for vacuum), g the gap width, h_{rad} the radiation heat transfer coefficient. The coefficient h_0 is the default heat transfer coefficient when no gap exists: h_0 is possibly related to the presence of a coating at the interface, its value being then given by the ratio of the coating material conductivity over the coating thickness. As regards mechanical contact between different domains, it is managed by an augmented Lagrange multiplier formulation [27].

The stress models available in PROCAST include a thermo-elastic-viscoplastic model of the Perzyna type [28], a thermo-elastic-plastic model (similar to Eq. (4)) and an elastic model for the cast part as well as a rigid body model for mould materials [29]. All material properties can be chosen temperature dependent or constant. In this comparison the rigid, linear elastic, and thermo-elastic-plastic models were used.

Isotropic and kinematic hardening models are available. For isotropic hardening a linear formulation and a power law formulation are available:

$$\sigma_{eq} = \sigma_y + H\varepsilon_{eq}^{pl} \text{ , respectively } \sigma_{eq} = \sigma_{00} + (\sigma_y - \sigma_{00})e^{-\beta\varepsilon_{eq}^{pl}} \tag{7}$$

H is the plastic modulus σ_{00} the ultimate stress, β the hardening exponent.

As for liquid-solid coupling, no stress simulation is performed when elements are fully liquid. The stress simulation is started when the fraction of solidified melt in an element exceeds a given limit.

Application of PROCAST to the benchmark test

The simulations were performed for one quarter of the geometry. One mesh consisting of tetrahedral elements (24 756 nodes, 136 391 elements, average characteristic size 3.4 mm) and another mesh consisting of brick and wedge elements (12 987 nodes, 11 700 elements, average characteristic size 5.4 mm) were used. For the pure heat transfer calculations in step 1, only the tetrahedral mesh was used. However, it was assured by a number of control simulations that use of tetrahedral and hexahedral meshes lead to the same results. Most of the simulations for the alloys Al-7%Si-0.3%Mg and Al-13%Si were performed using both meshes. The reported results of steps 2 and 3 are from the simulations using the mesh consisting of brick and wedge elements.

The stress models chosen for the simulations are: rigid for the core and the insulation, linear elastic for the mould and elastic-plastic for the melt. In the melt, the Ramberg-Osgood constitutive equation has been approached by an elastic-plastic law with linear hardening.

2.2.4. THERCAST

THERCAST® is a commercial finite element code that aims at the three-dimensional thermomechanical analysis of castings. The code is developed by CEMEF and TRANSVALOR and is focused on the calculation of deformations and stresses in the

castings, taking into account possible deformations in moulds. It includes a mould filling module permitting a possible initialisation of velocity and temperature fields, and an automatic meshing module [19].

Main features of the thermomechanical module of THERCAST

The module consists of a multidomain heat transfer solver, of enthalpy type, using linear temperature field in tetrahedral elements, and of a multidomain mechanical solver, based on a mixed velocity-pressure formulation [11, 30]. The mechanical contact between the different domains (the casting and the different components of the mould) is managed by a penalty-type algorithm [30, 31]. The heat transfer and the mechanical solvers are strongly coupled. At each time increment, a heat transfer and a mechanical resolution are performed. In the heat transfer solver, HTCs can depend locally on the size of the air gap or on the local contact pressure between two different domains. In the mechanical solver, the constitutive parameters are temperature dependent [30].

Regarding constitutive equations, the cast alloy can be considered either as a liquid-type or as a solid-type continuous medium, separated by a critical temperature T_C [30, 32, 33]. Above T_C a pure thermo-viscoplastic model is used. In this case, the compressibility is only due to the thermal contribution (no elasticity), as shown in Eq. (8). This is a classic power-law model for generalized non Newtonian fluids, and the associated one-dimensional relationship is given by Eq. (9). The limit case of the Newtonian behaviour is obtained for $m = 1$. In this case, $K = 3\eta$ with η the dynamic viscosity of the liquid alloy.

$$\dot{\bar{\bar{\varepsilon}}} = \dot{\bar{\bar{\varepsilon}}}^{vp} + \dot{\bar{\bar{\varepsilon}}}^{th} \qquad \dot{\bar{\bar{\varepsilon}}}^{vp} = \frac{3}{2K}(\dot{\varepsilon}_{eq}^{vp})^{1-m}\,\bar{\bar{s}} \qquad \dot{\bar{\bar{\varepsilon}}}^{th} = \left(\alpha\dot{T} + \tfrac{1}{3}\dot{f}_s\Delta\varepsilon^{tr}\right)\bar{\bar{I}} \tag{8}$$

$$\sigma_{eq} = K(\dot{\varepsilon}_{eq}^{vp})^{m} \tag{9}$$

Below T_C different thermo-elastic-viscoplastic models can be used. In this study, the model described by Eq. (10) has been chosen. Equation (10b) yields the hypoelastic Hooke's law, while (10c) gives the expression of the viscoplastic strain rate (the expression between brackets reduces to zero when negative: when σ_{eq} is lower than the plastic threshold $\sigma_y + H(\varepsilon_{eq}^{vp})^n$, no viscoplastic deformation occurs).

$$\begin{cases} \dot{\bar{\bar{\varepsilon}}} = \dot{\bar{\bar{\varepsilon}}}^{el} + \dot{\bar{\bar{\varepsilon}}}^{vp} + \dot{\bar{\bar{\varepsilon}}}^{th} \\ \dot{\bar{\bar{\varepsilon}}}^{el} = \dfrac{1+\nu}{E}\dot{\bar{\bar{\sigma}}} - \dfrac{\nu}{E}\mathrm{tr}(\dot{\bar{\bar{\sigma}}})\bar{\bar{I}} + \dot{T}\dfrac{\partial}{\partial T}\left(\dfrac{1+\nu}{E}\right)\bar{\bar{\sigma}} - \dot{T}\dfrac{\partial}{\partial T}\left(\dfrac{\nu}{E}\right)\mathrm{tr}(\bar{\bar{\sigma}})\bar{\bar{I}} \\ \dot{\bar{\bar{\varepsilon}}}^{vp} = \dfrac{3}{2\sigma_{eq}}\left\langle\dfrac{\sigma_{eq} - \sigma_y - H(\varepsilon_{eq}^{vp})^n}{K}\right\rangle^{1/m}\bar{\bar{s}} \\ \dot{\bar{\bar{\varepsilon}}}^{th} = \left(\alpha\dot{T} + \tfrac{1}{3}\dot{f}_s\Delta\varepsilon^{tr}\right)\bar{\bar{I}} \end{cases} \tag{10}$$

From this set of tensor equations, the one-dimensional law can be extracted:

$$\sigma_{eq} = \sigma_y + H(\varepsilon_{eq}^{vp})^n + K(\dot{\varepsilon}_{eq}^{vp})^m \quad (11)$$

The liquid-solid coupling is treated as follows. When solid-type, finite elements are Lagrangian (i.e. mesh velocity equals material velocity) whereas when liquid they are Eulerian-Lagrangian (mesh velocity is calculated independently of material velocity). This prevents mesh degeneracy in case of thermal convection, and allows the mesh boundary to follow the evolution of the free surface of the remaining liquid pool and then to model open shrinkage [32, 34].

Application of THERCAST to the benchmark test

To take advantage of the symmetry of the problem, the finite element meshes have been restricted to an angular sector of 11.25 degrees. The mesh size used in the part was about 2 to 3.5 mm in the part and 1 to 3 mm in the mould. Regarding constitutive equations, in order to compare with the other codes, only the solid-like constitutive model has been used (Eq. (10)-(11)) with coefficient K being null, in order to approach the Ramberg-Osgood strain-rate independent elastic-plastic model: parameters $H(T)$ and $n(T)$ have been identified to fit Eq. (3) on the whole temperature domain.

In THERCAST, the thermal linear expansion coefficient is deduced automatically from the primary data $\rho(T)$, given pointwise. For instance, in a finite element, α in Eq. (8) or (10) is defined as:

$$\alpha = \frac{-1}{3(T^{t+\Delta t} - T^t)} \frac{\rho(T^{t+\Delta t}) - \rho(T^t)}{\rho(T^t)} \quad (12)$$

where the specific mass is interpolated in the table $\rho(T)$. Because the shrinkage ratio $\Delta\varepsilon^{tr}$ is used, the coefficient α is set to zero in the solidification interval.

Automatic time step control has been applied for thermal and thermo-mechanical simulations with a maximum of 5 s.

3. RESULTS AND DISCUSSION

3.1. Step 1 computations : pure heat transfer with constant HTCs

As explained in Section 1, in this first step, the casting and the mould are considered rigid and the influence of the air gap on the heat transfer boundary conditions is ignored. Therefore only pure heat transfer is considered, with constant HTCs. This academic preliminary step serves as a comparison between the heat transfer solvers of the different numerical codes.

3.1.1. Al-7%Si-0.3%Mg alloy, step 1

It can be seen in Figure 5 that the results obtained with the different simulation codes are close.

In the core, the results from THERCAST slightly differ from the other ones (see Figure 5A, thermocouple located at r = 8 mm), but this can be attributed to a difference in the meshing. For meshing convenience, the core has not been meshed up to the axi-symmetrical axis. This perturbs the heating of the core, but has no further consequence because of the rapid heat saturation of the core that we have already mentioned in Section 1.

In the part, the cooling curves at the selected locations are very similar (Fig. 5B and C). A deeper examination of the results leads to the following remarks. Above the quasi-eutectic temperature of 561 °C, at which 93% of the alloy is solid, all results are included into a temperature interval of 6 °C. Below this temperature, the scatter interval tends to grow up to 24 °C. After complete solidification, the dispersion is maintained around a value of 20 °C.

Figure 5C illustrates the large difference between the calculated temperature and the measured one at the same location (mid-height of the specimen, radial co-ordinate 69 mm in the casting and 77 mm in the mould). This is clearly due to the choice of the constant HTC, the value of which has been chosen close to the maximum of the measured values. The decrease of the HTC due to gap opening, (Fig. 4B), is not taken into account and this leads to an overestimation of the heat extracted from the part. The temperature of the part is then underestimated by 80 to 90 °C. This clearly illustrates the crucial importance of the thermomechanical coupling in such simulations.

In the mould, all the results are included in an interval of 7 to 8 °C (Fig. 5D and E) and the overestimation of the heat exchange leads in this case to an overestimation of temperatures, by about 40 °C. In the experiment, the maximum of temperature happens much later than what is computed.

3.1.2. Eutectic Al-13%Si alloy, step 1

In the case of the eutectic alloy, the differences found between the results of the different codes are more significant, (Fig. 6). This is probably due to the sudden phase change associated with this eutectic alloy, which is more severe than for the previous alloy. This severely tests the different numerical algorithms used to treat the phase change.

First of all, the differences are found in the part (Fig. 6B and C), where two different groups of results appear: MAGMASOFT and THERCAST on one hand, CASTS and PROCAST on the other hand. The maximum scatter appears to be 25 °C before complete solidification of the casting and up to 45 °C after solidification. The results from CASTS appear to be affected by some kind of “stairway” effect due to the release of latent heat leading to numerical problems in a very small liquid/solid interval. As explained in [16], the apparent heat capacity method, although complemented by a post-iteration correction, might not be accurate enough in case of eutectic phase change.

Regarding the comparison with measured temperatures, the same conclusions can be drawn as for the previous alloy. The underestimation of temperatures in the casting varies from 60 to 90 °C, depending on which group of results is considered (Fig. 6C).

In the core and the mould, (Fig. 6A, D and E), the same differences logically appear between the codes, and between calculated and measured temperatures (mid-height of the specimen, radial co-ordinate 70.5 mm in the casting and 77 mm in the mould). Up to the end of

solidification, the same two groups of results can be identified. However, while CASTS and PROCAST show very similar results, MAGMASOFT show a more rapid cooling than the three other codes, and therefore progressively differ from THERCAST. The maximum temperature difference with the measurements is about 90 °C (Fig. 6D).

3.2. Step 2 computations : thermomechanical computations with time dependent HTCs

In the second step of the computations, the solidifying part and the mould deform and a thermomechanical computation is carried out on those two domains. The core and the insulation are assumed rigid. Between part and mould, a time dependent HTC deduced from experimental data is considered. As explained in Section 1, its value, which is assumed uniform on the whole interface, is directly deduced from the experimental measurements. So, there is no effective coupling from the mechanical calculation towards the heat transfer calculation. Only the coupling from the thermal calculation towards the mechanical calculation is taken into account through the temperature dependency of the part and mould constitutive parameters.

Because of this one-way coupling, the same trends as for step 1 can be observed for the cooling curves presented in Figures 7 and 8. Regarding part and mould displacements, it will be seen that there are big differences between the different codes.

3.2.1. Al-7%Si-0.3%Mg alloy, step 2

It can be seen on Figure 7 that the predicted temperature evolutions are in good agreement with the experimental measurements. This is quite normal since in this case the computations have used the HTCs directly deduced from experimental temperature measurements. Those coefficients have decreased due to gap formation (Fig. 4): consequently, the cooling of the part is slower than in step 1, and the heating of the mould is also slowed down after the initiation of the air gap, around 100 s. The temperature evolutions calculated by the different codes are very similar, as for step 1.

Regarding the mechanical side of the computations, Figure 7D shows the evolution of the displacement of the part and mould surfaces at the part/mould interface (r = 75 mm) at mid-height of the casting. The experimental curves are the same ones as in Figure 3B. They show the expansion of the mould, which stabilises at 400 s. At the beginning of the cooling, this expansion is followed by the part surface, up to 100 s which is the air gap formation time.

The mould expansion, which is governed by thermo-elasticity, is correctly predicted by the two codes that were able to take it into account: PROCAST and MAGMASOFT. It should be noted that the calculations done with CASTS-SPAN3D and THERCAST assumed a rigid mould. In the case of THERCAST, the software cannot treat time dependent HTCs and a 2D version of the code, named R2SOL, was used for step2, but permitting only rigid mould computations.

The comparisons of the different curves for displacement of the part show a huge dispersion. It can be seen that MAGMASOFT, CASTS-SPAN3D and THERCAST (R2SOL) show an immediate contraction of the alloy, but the amplitude and the time evolution of this deformation is totally different : it remains very small with MAGMASOFT, whereas the

evolution during the first 60 s is similar with CASTS-SPAN3D and THERCAST (R2SOL), but then becomes completely different: at 800 s, the gap predicted by CASTS-SPAN3D exceeds the experimental one by 150 % (around 900 μm instead of 600 μm) and the gap predicted by THERCAST is three times greater (around 1800 μm). PROCAST shows maybe the best (or least bad?) result, with an initial expansion of the alloy, following the mould, but with a too early gap formation by comparison with the experiment and a gap size twice bigger than the measured one: at 800 s, 1200 μm instead of 600 μm.

This dispersion of mechanical results can be caused by two different reasons:

- A primary source of errors is the Ramberg-Osgood law itself. It is an elastic-plastic constitutive equation which had been chosen for its simplicity, and because all the codes were able to compute it (or at least compute with an approaching elastic-plastic constitutive equation). However, it is well known that the constitutive equations of metallic alloys at high temperature are of elastic-viscoplastic type, including strain rate dependency. In addition, questions can be raised about the quality of the Ramberg-Osgood parameters that have been used. Those parameters were taken from the data base of MAGMASOFT. There is no doubt that their reliability is limited, especially at high temperature below the solidus. In mushy and liquid state, such an elastic-plastic model is certainly not relevant. All together, this might be a primary source of differences between computations and experience. However, it should be pointed out that this does not explain why the different computations are so different.
- The Ramberg-Osgood constitutive law has been entered differently in the codes. Except for MAGMASOFT, the law is not directly available in the codes and a fitting has been done by each user to approach as best as possible the stress-strain curves at different temperatures with other constitutive models such as power law models for instance (see Section 2.2). It was impossible to do a cross-checking of the different curve fittings in order to be sure that they were all reliable and of the same quality. This is obviously a source of differences between the different computations, which can be enhanced by possible errors done when writing the data files for the different simulation codes.

3.2.2. Eutectic Al-13%Si alloy, step 2

The results from the calculations of Al-13%Si are given in Figure 8. Looking at temperature curves (Fig. 8A to C), we notice some dispersion between the results, as for the computations of step 1 for the same alloy. However, the situation is different. Now PROCAST and THERCAST give very similar results, whereas CASTS-SPAN3D shows a more rapid cooling and MAGMASOFT a longer one. This is surprising because, regarding the thermal computations, the only difference between step 1 and step 2 computations lies in the fact that in step 2, the HTCs are time dependent. As for Al-7%Si-0.3%Mg, it can be seen that the predicted temperature evolutions are in reasonable agreement with the experimental measurements. From this point of view, CASTS-SPAN3D provides the best result.

A great scattering can again be noticed in the results for the displacements (Fig. 8D). The mould expansion is rather well modelled by MAGMASOFT and PROCAST. PROCAST and THERCAST (R2SOL) show a very rapid contraction of the part. The part displacement is first

different and then becomes quite similar for higher process times. The values are highly overestimated with respect to the measurements. The MAGMASOFT computations show no displacement at all of the part until 300 s, and then a contraction with values that are comparable to the measured ones. No results are shown for CASTS-SPAN3D because the mechanical computation of the code failed in this case.

3.3. Step 3 computations : fully coupled thermomechanical computations

In the third and last step of the comparison, thermomechanical computations have been carried out in which the value of the HTC between part and mould depends locally on the size of the air gap. Unlike step 2, the mechanical calculation has now an influence on the heat transfer calculation. Only two codes, PROCAST and THERCAST permitted such fully coupled thermomechanical computations.

Using PROCAST, the HTC is determined according to Eq. (6).

Using THERCAST, the gap size dependency of the HTC has been established in the following manner. From the measured gap size evolution $g(t)$ (Fig. 3) and from the measured HTC $h(t)$ (Fig. 4), it was possible to deduce the intrinsic gap size dependency of the HTC $h(g)$. This relation was introduced stepwise in the data file of the code. When solving the heat transfer problem, the local gap size is known (from the mechanical module), and therefore the appropriate local value of h is deduced from the table $h(g)$ by linear interpolation.

3.3.1. Al-7%Si-0.3%Mg alloy, step 3

It can be seen in Figure 9A to C that the predicted cooling of the part is much slower in this case. The solidification time predicted by PROCAST is approximately twice as large as the measured one, whilst THERCAST shows a very slow cooling down: the part is still not solidified after 1000 s. Accordingly, the heating of the mould (Fig. 9C) is considerably reduced as compared to step 2 for example. The cause of this behaviour can be found in the examination of the displacement curves (Fig. 9D). Both codes predict a gap size that is greater than the measured one (much greater in the case of THERCAST) and consequently the values of h are overestimated, leading to underestimated heat fluxes at the interface between part and mould. From the mould side, we can see that its expansion is limited compared to step 2 computations, because of reduced heating.

As for step 2, the same reasons explain these results.

3.3.2. Eutectic Al-13%Si alloy, step 3

In this case the mechanical module of PROCAST failed to perform a calculation. In Figure 10, only THERCAST results are given, showing the same trend as with the Al-7%Si-0.3%Mg alloy.

3.4. Additional results using a liquid/solid approach

In order to overcome the limitations and inaccuracies coming from the use of an elastic-plastic constitutive equation (see the discussion in Section 3.2.1), complementary

computations have been carried out with THERCAST software, in the case of Al-7%Si-0.3%Mg alloy. As described in Section 2.2.4, liquid-like and solid-like constitutive equations are distinguished and used simultaneously in the simulation. Above the temperature T_C, here chosen equal to 569 °C (corresponding to the eutectic temperature at $f_s = 0.77$) the material is considered as viscoplastic (Newtonian over T_L), whereas it obeys an elastic-viscoplastic model below T_C. Instead of Eq. (10c), a multiplicative-type expression has been chosen for the viscoplastic strain-rate tensor:

$$\bar{\bar{\dot{\varepsilon}}}^{vp} = \frac{3}{2\sigma_{eq}} \left\langle \frac{\sigma_{eq} - \sigma_y}{K(\varepsilon_{eq}^{vp})^n} \right\rangle^{1/m} \bar{\bar{s}} \tag{13}$$

yielding:

$$\sigma_{eq} = \sigma_y + K(\varepsilon_{eq}^{vp})^n (\dot{\varepsilon}_{eq}^{vp})^m \tag{14}$$

The temperature dependent parameters of these constitutive equations are given in Table 2. All other data are the same. Comparing Figure 11 to Figure 9, it can be seen that the results are in better agreement with the experimental measurements. A comparison between Figures 11D and 9D especially shows that the motion of the casting is better represented with THERCAST when using the elastic-viscoplastic constitutive equations. The maximum error on the part displacement is about 0.15 mm in this case, whereas it is as high as 0.6 mm using elasto-plasticity. This more realistic part displacement yields a reasonably good gap size prediction (Figure 11E), which in turn leads to a better estimation of the heating of the mould (Fig. 11C, which can be compared to Figure 9C), and of the cooling of the part (Fig. 11B, to be compared with Figure 9B). In addition, it is interesting to compare the shape of the part that is obtained using the two approaches: see Figure 12. Using the first elastic-plastic approach, the part appears to shrink rather uniformly, with a large air gap and a flat free surface at the top. In our opinion, this comes from the use of an elastic-plastic constitutive equation that is too stiff to model the flow of liquid and mushy material. Conversely, using the liquid/solid approach, the gap as already said is much smaller and the free surface shows a curved free surface which is in qualitative agreement with the experiment.

CONCLUSIONS

In this paper the simulations performed by four different numerical codes have been compared with reference to experimental measurements for two aluminium alloy castings with the same ring-type geometry. The main conclusions of this work are the followings.

- The responses of the different software in the case of pure heat transfer computation has been found quite similar, except in the case of the eutectic alloy for which the scattering of the results is important.
- Regarding the evaluation of the ability to predict air gap formation using coupled thermo-mechanical computations, it was difficult to perform a complete comparison between

codes, mainly for two reasons. First, among the four codes considered, only two were able to address a fully coupled thermo-mechanical problem, in which the air gap formation locally modifies the heat transfer. Second, it was difficult to determine a constitutive equation that could be accepted by all four codes.

- There is still a considerable lack of knowledge regarding the mechanical constitutive equations, and their associated parameters, to be used in solidification conditions. This obviously needs further work. In the meantime, the limitations of the use of oversimplified behaviour laws such as elasto-plasticity over too wide temperature intervals, including liquid and mushy states, have been demonstrated.
- The results from this work also give a reason to look more thoroughly into the numerical treatment of solidification shrinkage. All four programs consider the shrinkage to contribute to the air gap formation; either by adding a term to the thermal contraction in the expression for thermal strain, or by adjusting the thermal expansion coefficient. However, the results from step 2 in this work show that with the use of the thermal data from these experiments, the prediction of the air gap done with the computer programs is not satisfactory. There is also experimental support as to why the solidification shrinkage should be relaxed by the melt and therefore contribute to a cavity in the top of the casting or porosity, rather than affecting the air gap. One example of such an experimental observation is the positive segregation that is observed near the surface towards the cool side of a casting, showing that a relaxation of the shrinkage is actually taking place. The conclusion must be that the model for describing the total strain in a solidifying material needs to be defined more carefully.

ACKNOWLEDGEMENTS

This paper is an outcome of the EU-network “Microstructural Engineering By Solidification Processing (MEBSP)”, subgroup 4 “Thermal stresses and strains during solidification”. The authors wish to express their gratitude for financial support by the European Commission.

REFERENCES

[1] L.J.D. Sully, ”The thermal interface between castings and molds”, *AFS Trans.*, 1976, 735-744.

[2] K. Ho and R.D. Pehlke, ”Metal-mold interfacial heat transfer”, *Metall. and Mat. Trans. B*, 1985, 585-594.

[3] K. Ho and R.D. Pehlke, ”Transient methods for determination of metal-mold interfacial heat transfer”, *AFS Trans.*, 1983, 689-698.

[4] J. Isaac, G.P. Reddy and G.K. Sharma, ”Variations of heat transfer coefficients during solidification of castings in metallic moulds”, *The British Foundryman*, 1985, 465-468.

[5] W.D. Griffiths, ”The heat transfer coefficient during the unidirectional solidification of an Al-Si alloy casting”, *Metall. and Mat. Trans. B*, 1999, 30, 473-482.

[6] K.N. Prabhu and J. Campbell, ”Investigation of casting/chill interfacial heat transfer during solidification of Al-11%Si alloy by inverse modelling and real time X-ray imaging”, *Int. J. Cast Metals Res.*, 1999, 12, 137-143.

[7] B.P. Winter and R.D. Pehlke, ”Volumetric shrinkage and gap formation during solidification of copper-base alloys”, *AFS Trans.*, 1983, 81-88.

[8] K. Ho and R.D. Pehlke, ”Mechanisms of heat transfer at a metal-mold interface*”, AFS Trans.*, 1984, 587-598.

[9] J.G. Henzel and J. Keverian, ”Gap formation in permanent mold castings”, *Trans. of the American foundrymen´s society*, 1960, 68, 373-379.

[10] Y. Nishida, W. Droste and S. Engler, ”The air gap formation process at the casting-mold interface and the heat transfer mechanism through the gap”, *Metall. and Mat. Trans. B*, 1986, 833-844.

[11] M. Bellet, F. Decultieux, M. Ménaï, F. Bay, C. Levaillant, J-L. Chenot, P. Schmidt and I.L. Svensson, ”Thermomechanics of the cooling stage in casting processes: three-dimensional finite element analysis and experimental validation”*, Metall. and Mat. Trans. B*, 1996, 27, 81-99.

[12] F. Decultieux, M. Ménaï, F. Bay, C. Levaillant, P. Schmidt, I.L. Svensson and M. Bellet, “Thermomechanical modeling in casting with experimental validation”, *Modelling in Welding, Hot Powder Forming and Casting*, L. Karlsson (ed.), ASM International, 1997, chap. 10, 291-313.

[13] Z.H. Lee, T.G. Kim and Y.S. Choi, ”The movement of the concave casting surface during mushy-type solidification and its effect on the heat transfer coefficient”, *Metall. and Mat. Trans. B*, 1998, 29, 1051-1056.

[14] M. Trovant and S.A. Argyropoulos, ”The implementation of a mathematical model to characterize mold metal interface effects in metal casting”*, Canadian Metall. Quarterly*, 1998, 37, 185-196.

[15] O. Richmond and R.H.Tien, "Theory of thermal stresses and air-gap formation during the early stages of solidification in a rectangular mold", *J. Mech. Solids*, 1971, 19, 273-284.

[16] G. Laschet, J. Neises and I. Steinbach, "Micro and Macrosimulation of Casting Processes", Lecture Notes of 4ème Ecole d'été du CNRS, Porquerolles, France, 1998, published by Editions du CNRS, 1998, chap. C8, 1-42.

[17] http://www.magmasoft.com

[18] http://www.calcom.ch/Products/Procast.html

[19] THERCAST presentation on www.transvalor.com/ and www.scconsultants.com/

[20] P. Schmidt, *Heat transfer and air gap formation in permanent mould casting of aluminium alloys*, Ph.D. Thesis, Trita-Mac-0541, The Royal Institute of Technology, Stockholm, Sweden, 1994.

[21] J. Kron, T. Antonsson and H. Fredriksson, "Air gap formation during solidification in cylindrical castings of pure aluminium and eutectic Al-Si", *Int. J. Cast Metals Res.*, 2002, 14, 275-285.

[22] J. Kron and H. Fredriksson, "Air gap formation during solidification of aluminium base alloys in a permanent mould", Proc. ASM Materials Solutions Conference and Exposition 2002, October 7-10, Columbus, Ohio, USA, published by ASM International, Ohio, USA, 2002.

[23] W. Ramberg and W.R. Osgood, "Determination of Stress-strain Curves by Three Parameters", Technical Note No. 503, National Advisory Committee on Aeronautic NACA, (1941)

[24] W.R. Osgood, "Stress-strain formulas", *J. Aeronaut. Sci*., 1946, 13, 45-48.

[25] J. Guan, Ph.D. Thesis, Technical University (RWTH), Aachen, Germany, 1994.

[26] http://www.ues-software.com/

[27] J.C. Simo and T.A. Laursen, "An Augmented Lagrangian Treatment of Contact Problems Involving Friction", *Comput. Struct.*, 1992, 42, 97-116.

[28] P.Perzyna, "Fundamental Problems in Viscoplasticity", *Adv. Appl. Mech.*, 1966, 9, 243-377.

[29] M. Samonds, Z.J. Zhong, "Coupled Thermal-fluids-stress Analysis of Castings", *Proc. 9th Int. Conf. on Modeling of Casting, Welding and Advanced Solidification Processes*, Aachen (Germany), 2000, P.R. Sahm, P.N. Hansen, J.G. Conley (eds.), Shaker Verlag, Aachen, 2000, 80-87.

[30] O. Jaouen, *Modélisation tridimensionnelle par éléments finis pour l'analyse thermomécanique du refroidissement des pièces coulées* (*Three-dimensional finite element modelling for thermomechanical analysis of the cooling of cast parts*), Ph.D. Thesis (in french), Ecole des Mines de Paris, 1998.

[31] O. Jaouen and M. Bellet, "A numerical mechanical coupling algorithm for deformable bodies: application to part/mold interaction in casting process", *Proc. 8th Int. Conf. on*

Modelling of Casting, Welding and Advanced Solidification Processes, San Diego (CA, USA), 1998, B.G. Thomas and C. Beckermann. (eds.), The Minerals Metals and Materials Society, 1998, 739-746.

[32] M. Bellet and O. Jaouen, "Finite element approach of thermomechanics of solidification processes", *Proc. Int. Conf. On Cutting Edge of Computer Simulation of Solidification and Casting*, Osaka (Japan), 1999, I. Ohnaka and H. Yasuda (eds.), The Iron and Steel Institute of Japan (ISIJ), 1999, 173-190.

[33] M. Bellet, C. Aliaga and O. Jaouen, "Finite elements for a thermomechanical of analysis of solidification processes", *Proc. 9th Int. Conf. on Modeling of Casting, Welding and Advanced Solidification Processes*, Aachen (Germany), 2000, P.R. Sahm, P.N. Hansen and J.G. Conley (eds.), Shaker Verlag, Aachen, 2000, 10-17.

[34] M. Bellet, O. Jaouen and I. Poitrault, "An ALE-FEM Approach to the thermomechanics of solidification processes with application to the prediction of pipe shrinkage", to be published in *Int. J. Num. Meth. for Heat & Fluid Flow*.

TABLES AND FIGURES

Table 1: Constant values for the heat transfer coefficient between part and mould for step 1 computations.

Table 2: Rheological properties of Al-7%Si-0.3%Mg used in THERCAST computation. For confidentiality reasons, actual values cannot be given. Typical values are given and the interpolation between the given values should not been assumed linear.

Figure1: Geometry of the experimental set-up.

Figure 2: Cooling curves from the experiments A: eutectic alloy Al-13%Si (measurement at r = 70.5 mm in the casting and at r = 77 mm in the mould), B: Al-7%Si-0.3%Mg (measurement at r = 69 mm in the casting and at r = 77 mm in the mould).

Figure 3: Measured radial displacements in experiments A: eutectic alloy Al-13%Si, B: Al-7%Si-0.3%Mg. In both charts, the inner surface of the mould has a positive radial displacement while the surface of the casting has a negative one.

Figure 4: Calculated heat transfer coefficients for the experiments. A: eutectic alloy Al-13%Si, B: Al-7%Si-0.3%Mg.

Figure 5: Results for step 1 Al-7%Si-0.3%Mg alloy. Pure heat transfer calculations with constant heat transfer coefficients.

Figure 6: Results for step 1 Al-13%Si alloy. Pure heat transfer calculations with constant heat transfer coefficients.

Figure 7: Results for step 2 Al-7%Si-0.3%Mg alloy. Thermomechanical calculations with time dependent heat transfer coefficients.

Figure 8: Results for step 2 Al-13%Si alloy. Thermomechanical calculations with time dependent heat transfer coefficients.

Figure 9: Results for step 3 Al-7%Si-0.3%Mg alloy. Thermomechanical calculations with gap dependent heat transfer coefficients.

Figure 10: Results for step 3 Al-13%Si alloy. Thermomechanical calculations with gap dependent heat transfer coefficients.

Figure 11: Results for step 3 Al-7%Si-0.3%Mg alloy. Thermomechanical calculations with gap dependent heat transfer coefficients, using a liquid-solid constitutive model in THERCAST.

Figure 12: Results for step 3 Al-7%Si-Mg alloy. System configuration at 1000 s, computed with THERCAST. Left: Ramberg-Osgood elasto-plastic constitutive model. Right: distinction between fluid-like constitutive model (Newtonian/viscoplastic) and solid-like constitutive model (elastic-viscoplastic).

Table 1: Constant values for the heat transfer coefficient between part and mould for step 1 computations.

Alloy	$h_{casting/mould}$
Al-13%Si	1320 W m^{-2} K^{-1}
Al-7%Si-0.3%Mg	898 W m^{-2} K^{-1}

Table 2: Rheological properties of Al-7%Si-0.3%Mg used in THERCAST computation. For confidentiality reasons, actual values cannot be given. Typical values are given and the interpolation between the given values should not been assumed linear.

Elasto-viscoplasticity, below critical temperature T_C = 569 °C

Temperature [°C]	Consistency K [MPa]	Strain rate sensitivity coefficient m [-]	Hardening coefficient n [-]	Static yield stress σ_y [MPa]	Young modulus E [MPa]
20	2000	0.005	1.0	145	68000
200	230	0.01	0.7	140	65000
400	22	0.07	0.6	45	43000
542 (= T_S)	15	0.25	0.1	10	13000
569	0.2	0.3	0.0	0	300

Viscoplasticity, over critical temperature T_C = 569 °C

Temperature [°C]	Consistency K [MPa]	Strain rate sensitivity coefficient m [-]
569	0.2	0.3
613 (= T_L)	3×10^{-3}	1.0
800	3×10^{-3}	1.0

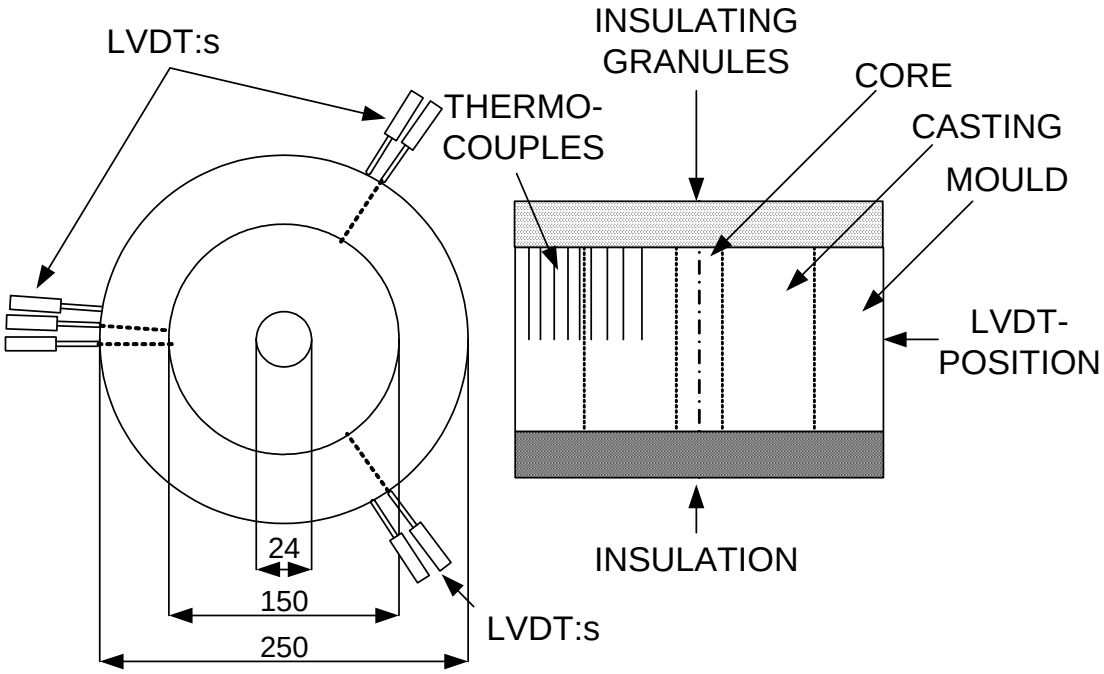

Figure 1: Geometry of the experimental set-up.

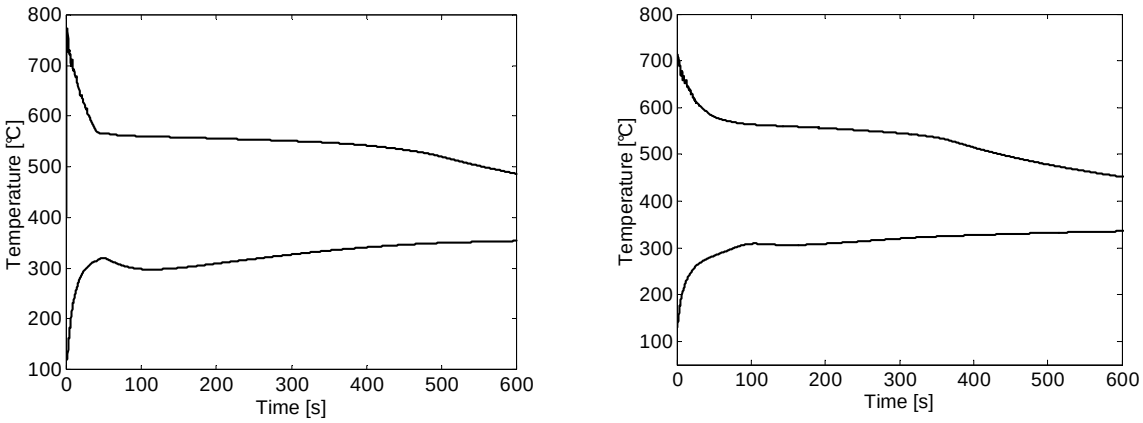

A *B*

Figure 2: Cooling curves from the experiments A: eutectic alloy Al-13%Si (measurement at r = 70.5 mm in the casting and at r = 77 mm in the mould), B: Al-7%Si-0.3%Mg (measurement at r = 69 mm in the casting and at r = 77 mm in the mould).

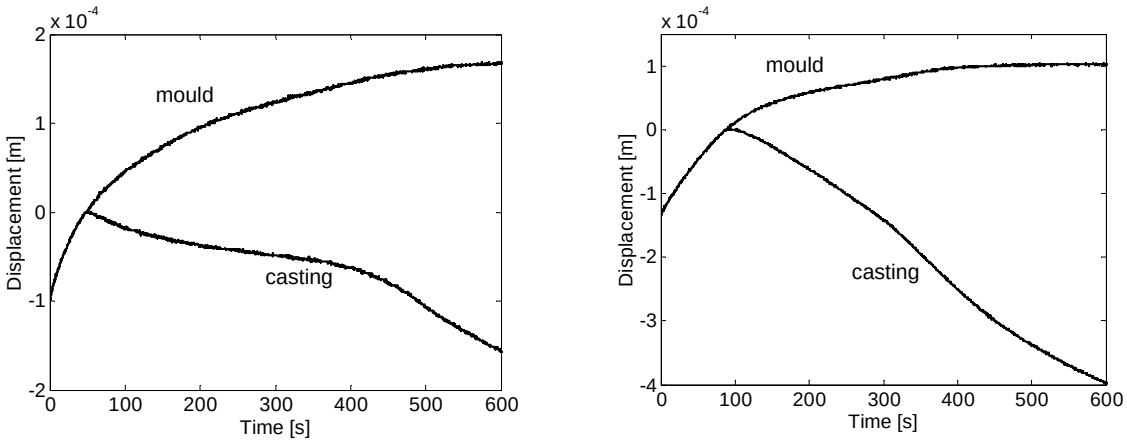

A *B*

Figure 3: Measured radial displacements in experiments A: eutectic alloy Al-13%Si, B: Al-7%Si-0.3%Mg. In both charts, the inner surface of the mould has a positive radial displacement while the surface of the casting has first a positive one, following the mould motion, and then a negative one due to solidification shrinkage.

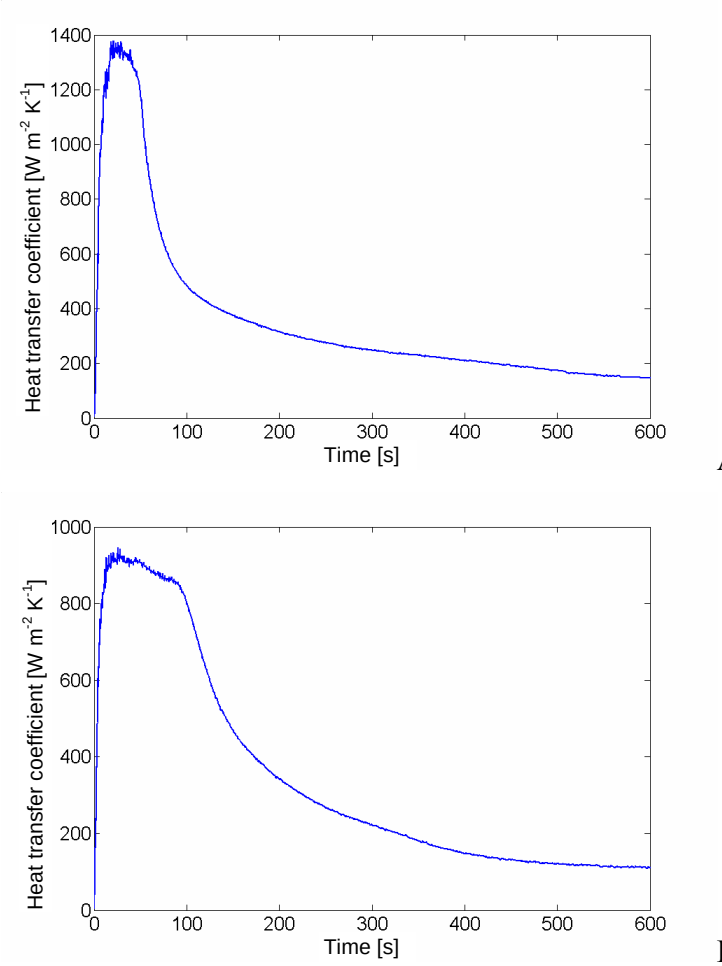

Figure 4: Calculated heat transfer coefficients for the experiments. A: eutectic alloy Al-13%Si, B: Al-7%Si-0.3%Mg.

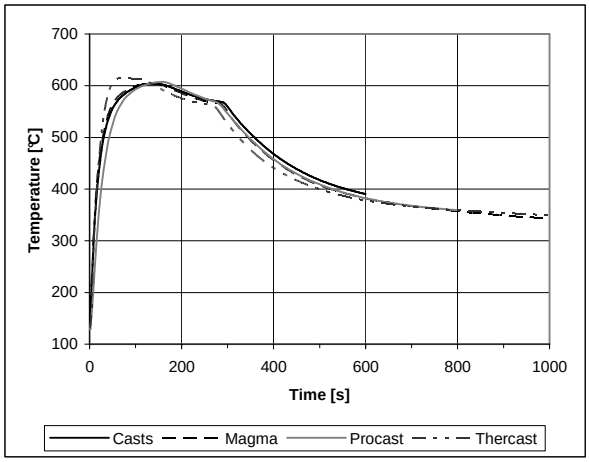

A: temperature in core at r = 8 mm

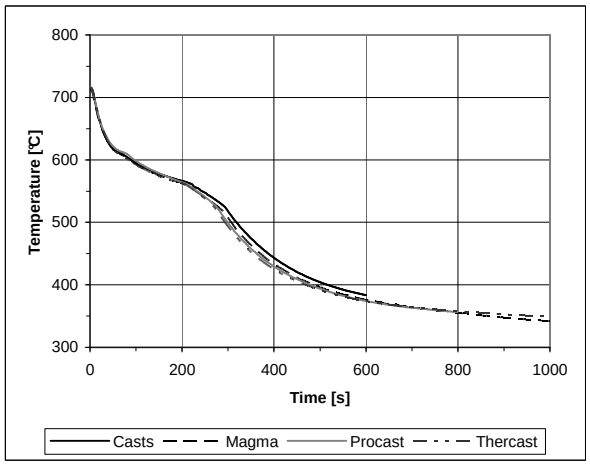

B: temperature in part at r = 45 mm

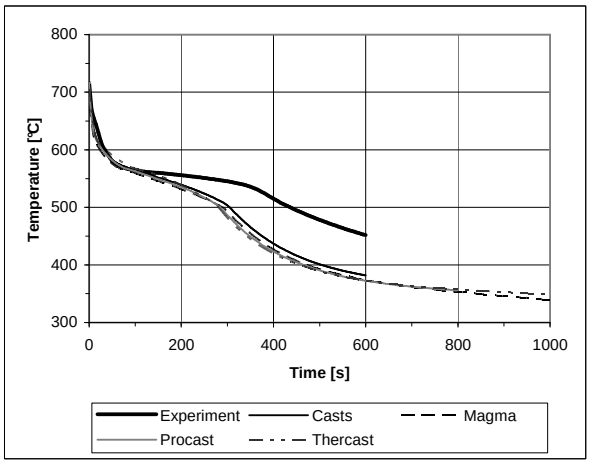

C: temperature in part at r = 69 mm

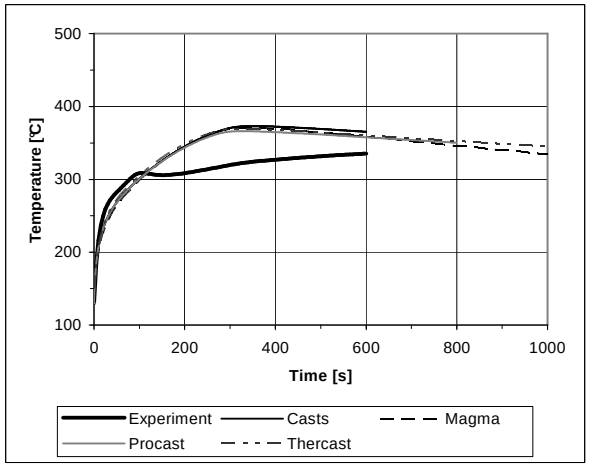

D: temperature in mould at r = 77 mm

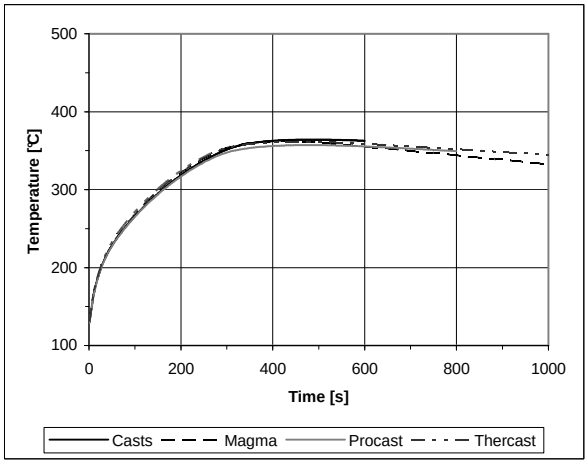

E: temperature in mould at r = 85 mm

Figure 5: Results for step 1 Al-7%Si-0.3%Mg. Pure heat transfer calculations with constant heat transfer coefficients.

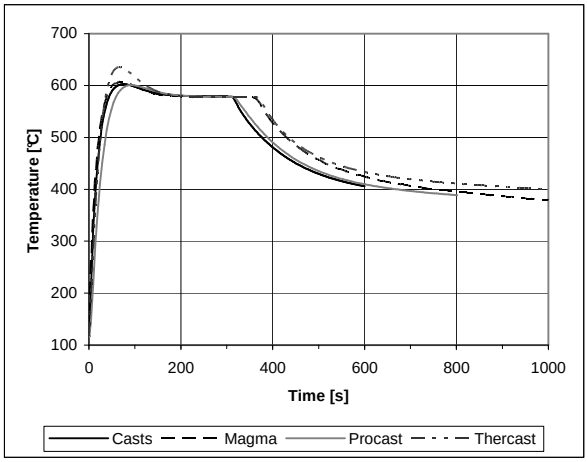

A: temperature in core at r = 8 mm

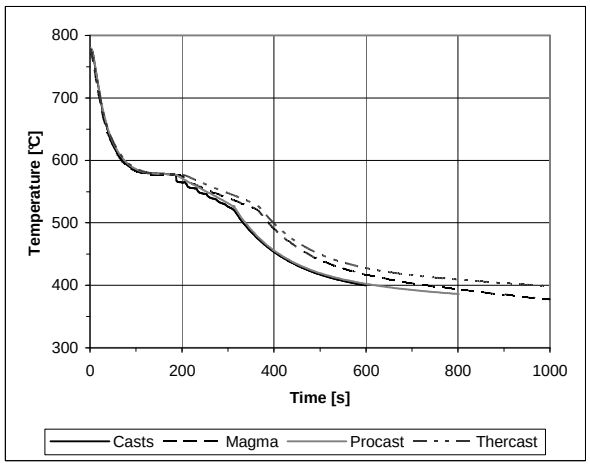

B: temperature in part at r = 45 mm

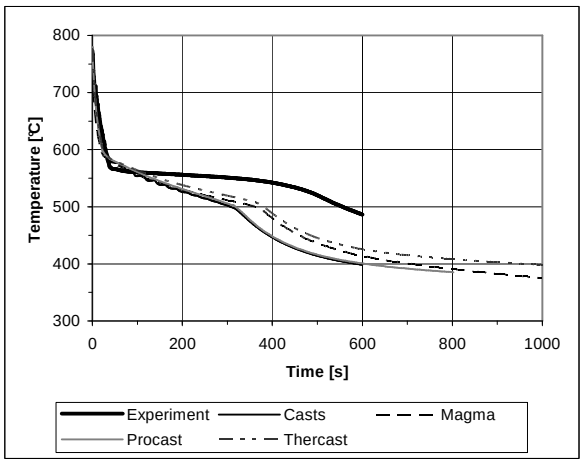

C: temperature in part at r = 70.5 mm

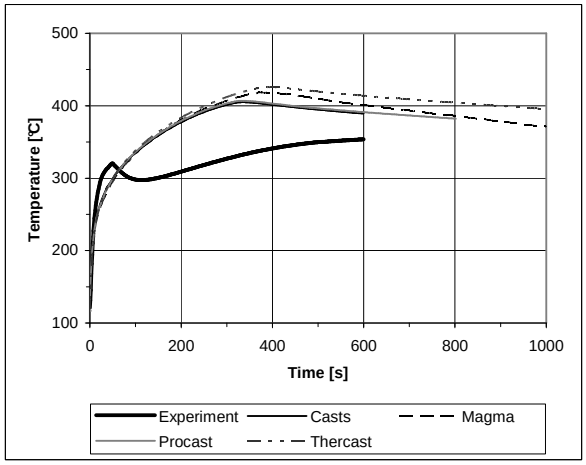

D: temperature in mould at r = 77 mm

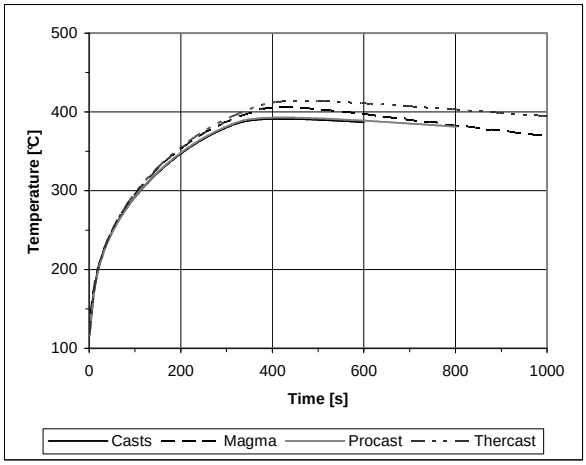

E: temperature in mould at r = 85 mm

Figure 6: Results for step 1 Al-13%Si. Pure heat transfer calculations with constant heat transfer coefficients.

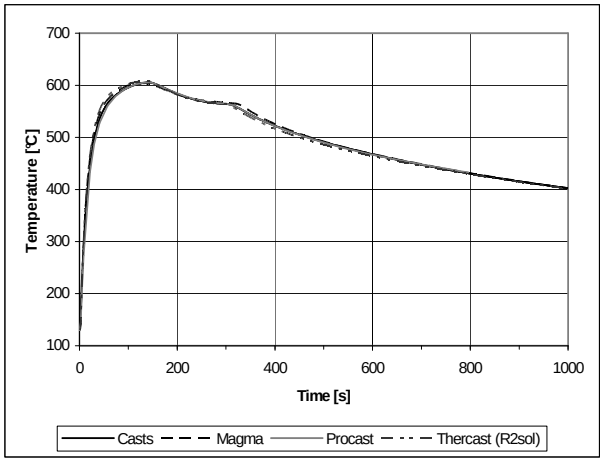

A: temperature in core at r = 8 mm

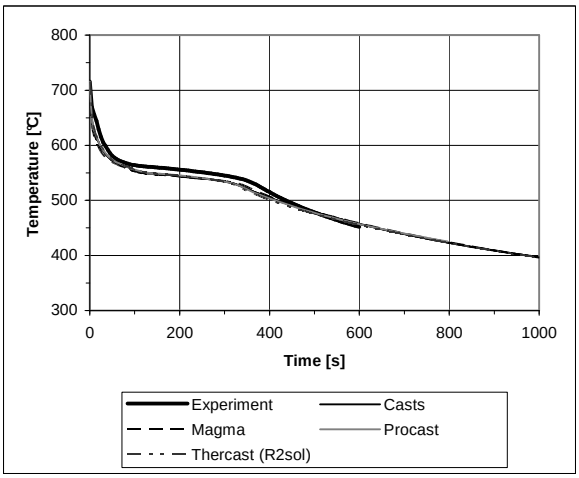

B: temperature in part at r = 69 mm

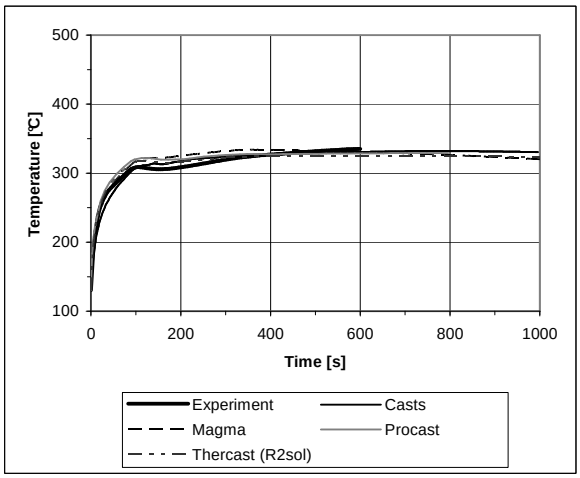

C: temperature in mould at r = 77 mm

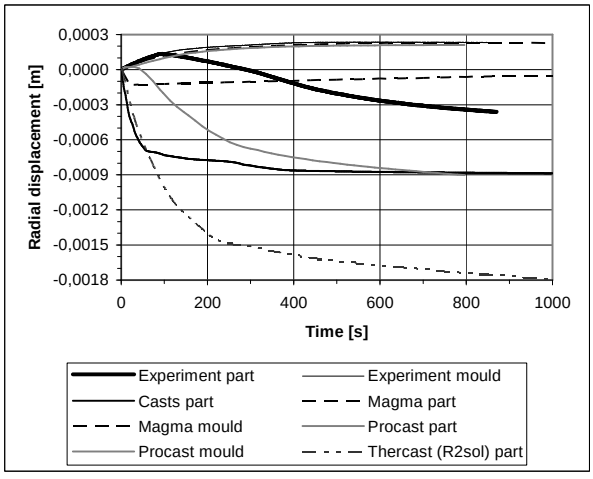

D: part and mould displacements

Figure 7: Results for step 2 Al-7%Si-0.3%Mg. Thermomechanical calculations with time dependent heat transfer coefficients.

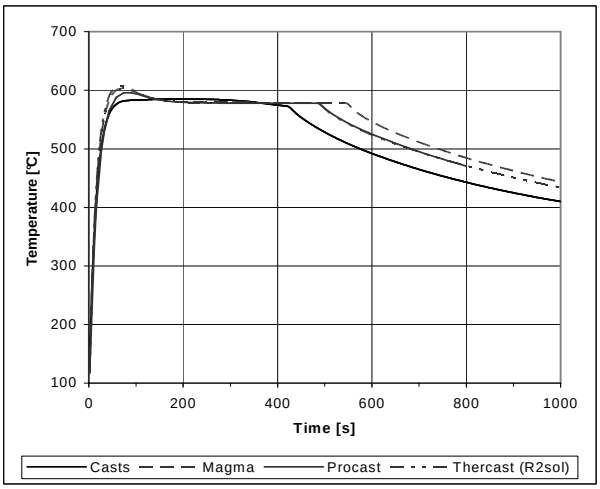

A: temperature in core at r = 8 mm

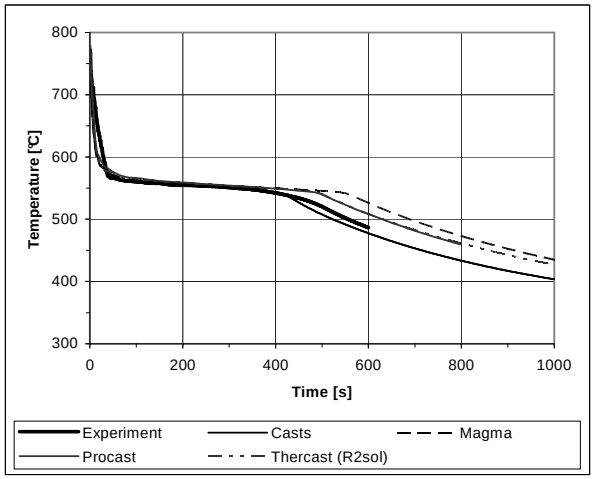

B: temperature in part at r = 70.5 mm

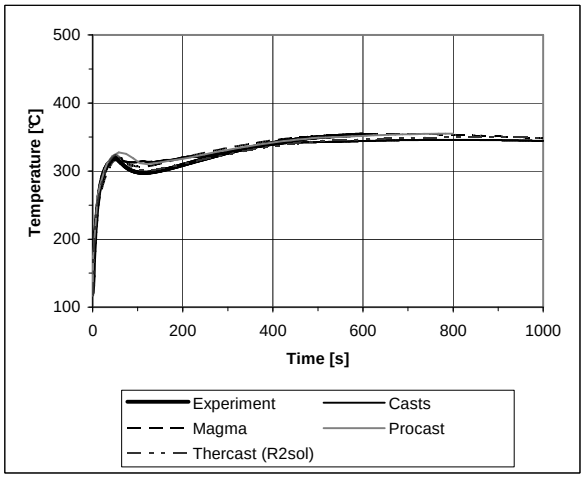

C: temperature in mould at r = 77 mm

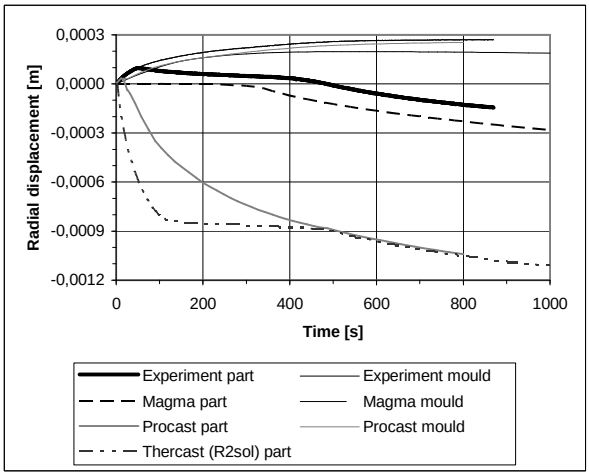

D: part and mould displacements

Figure 8: Results for step 2 Al-13%Si. Thermomechanical calculations with time dependent heat transfer coefficients.

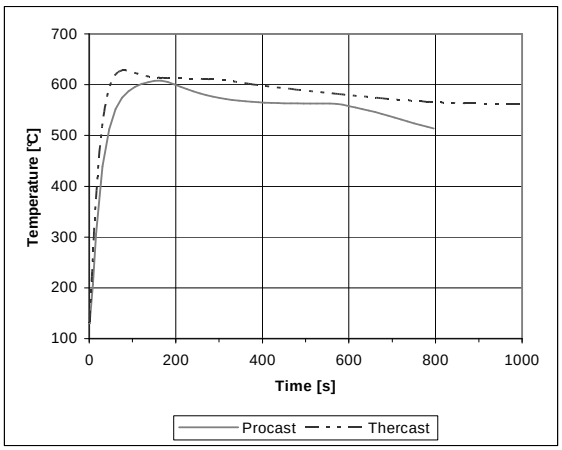

A: temperature in core at r = 8 mm

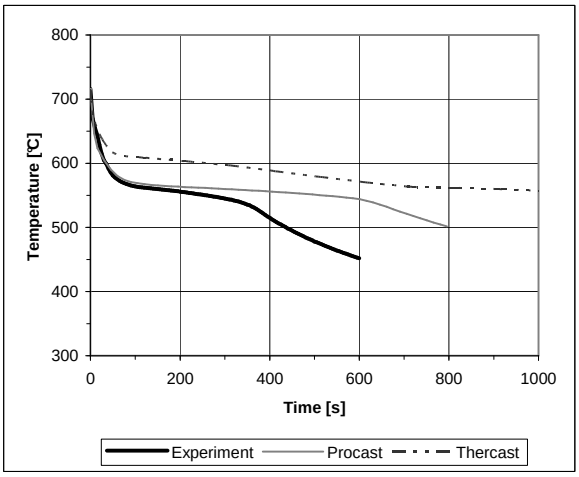

B: temperature in part at r = 69 mm

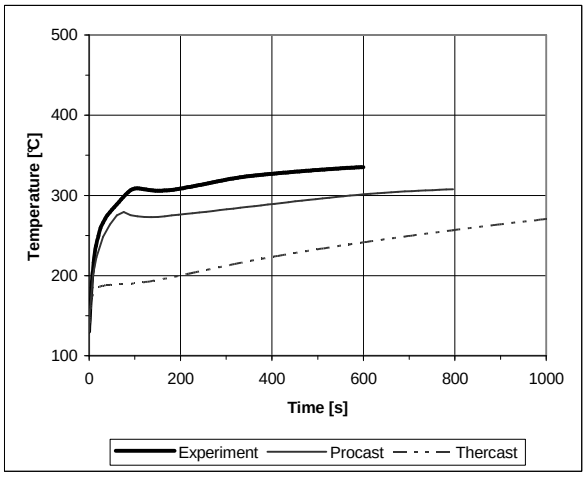

C: temperature in mould at r = 77 mm

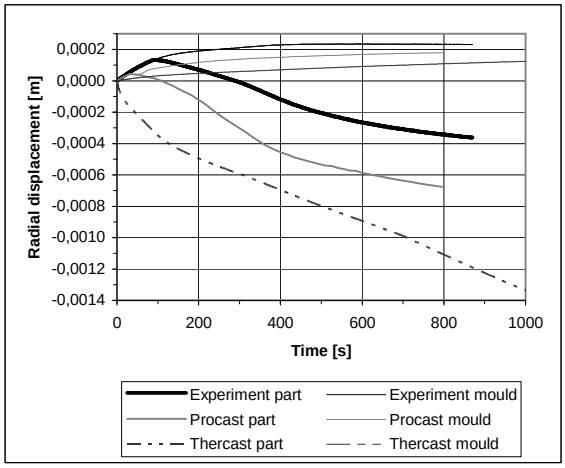

D: part and mould displacements

Figure 9: Results for step 3 Al-7%Si-0.3%Mg. Thermomechanical calculations with gap dependent heat transfer coefficients.

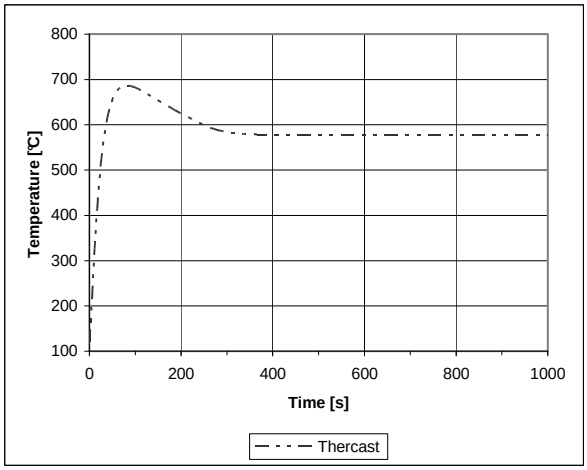

A: temperature in core at r = 8 mm

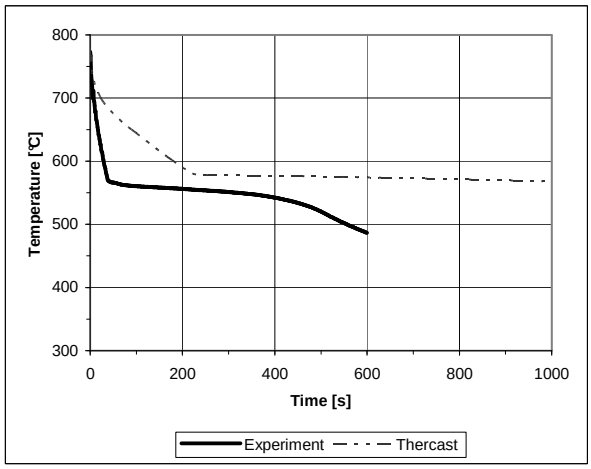

B: temperature in part at r = 70.5 mm

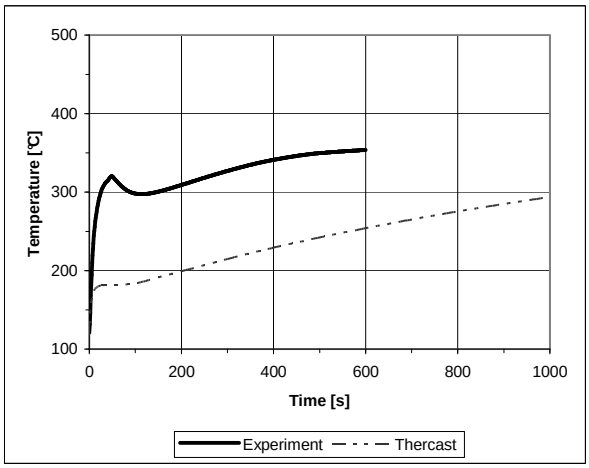

C: temperature in mould at r = 77 mm

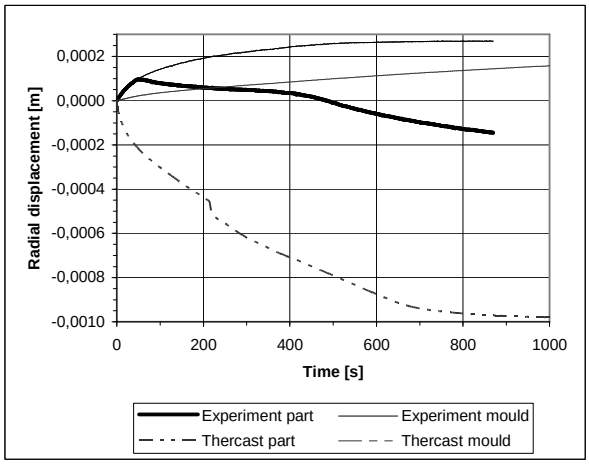

D: part and mould displacements

Figure 10: Results for step 3 Al-13%Si. Thermomechanical calculations with gap dependent heat transfer coefficients.

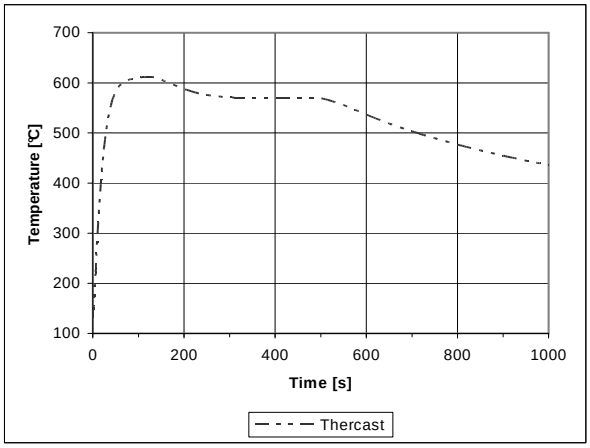

A: temperature in core at r = 8 mm

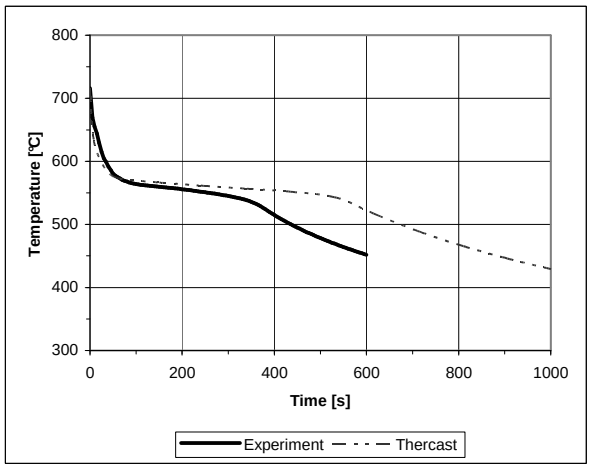

B: temperature in part at r = 69 mm

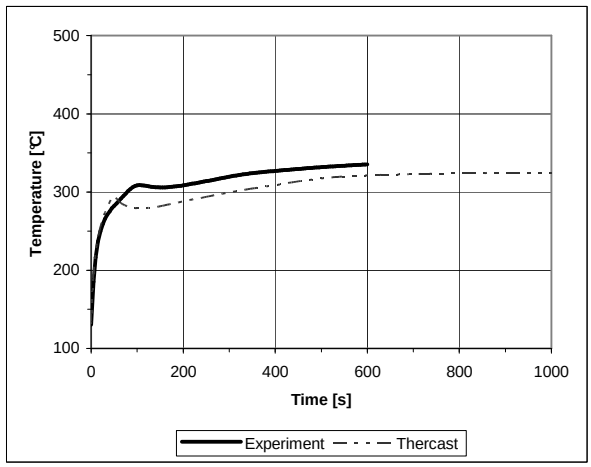

C: temperature in mould at r = 77 mm

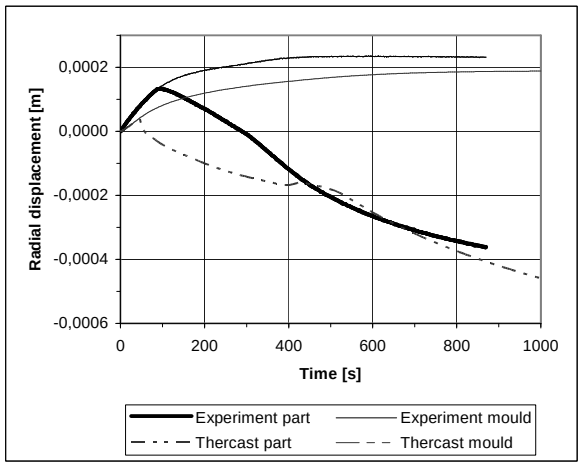

D: part and mould displacements

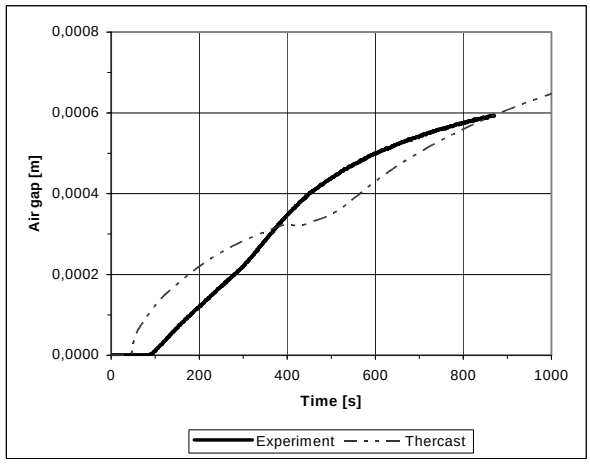

E: associated air gap evolution

Figure 11: Results for step 3 Al-7%Si-0.3%Mg. Thermomechanical calculations with gap dependent heat transfer coefficients, using a liquid-solid constitutive model in THERCAST.

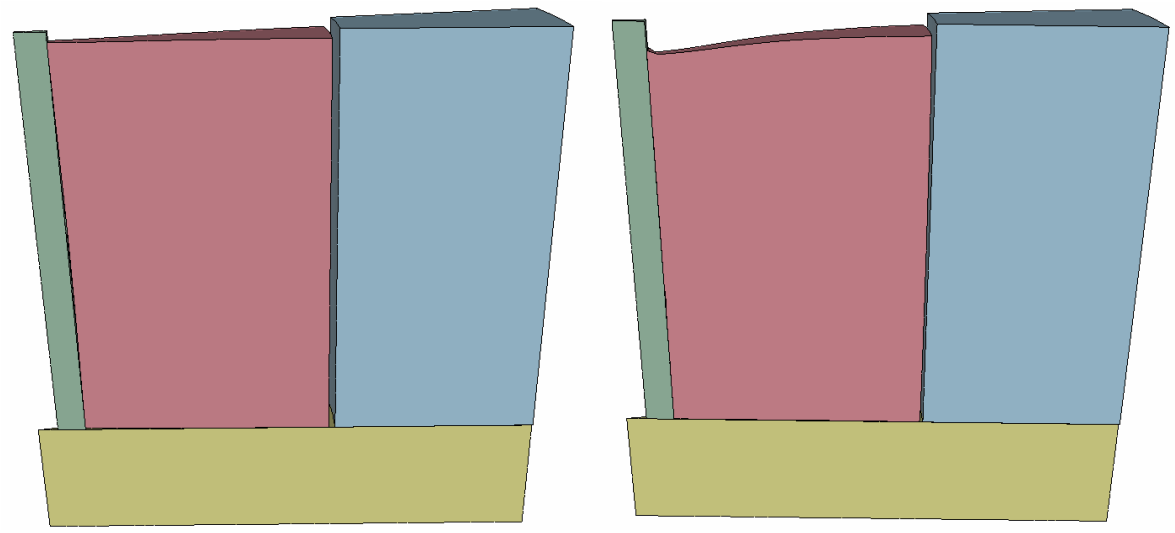

Figure 12: Results for step 3 Al-7%Si-Mg. System configuration at 1000 s, computed with THERCAST. Left: Ramberg-Osgood elasto-plastic constitutive model. Right: distinction between fluid-like constitutive model (Newtonian/viscoplastic) and solid-like constitutive model (elastic-viscoplastic).